JACS
JOURNAL OF THE AMERICAN CHEMICAL SOCIETY
Article
pubs.acs.org/JACS

Formation of Guanine-6-sulfonate from 6-Thioguanine and Singlet Oxygen: A Combined Theoretical and Experimental Study

Xiaoran Zou, Hongmei Zhao, Youqing Yu, and Hongmei Su*

Beijing National Laboratory for Molecular Sciences (BNLMS), State Key Laboratory of Molecular Reaction Dynamics, Institute of Chemistry, Chinese Academy of Sciences, Beijing 100190, People's Republic of China

Supporting Information

ABSTRACT: As an end metabolism product of the widely used thiopurine drugs, 6-thioguanine (6-TG) absorbs UVA and produces $^1O_2$ by photosensitization. This unusual photochemical property triggers a variety of DNA damage, among which the oxidation of 6-TG itself by $^1O_2$ to the promutagenic product guanine-6-sulfonate (G^{SO3}) represents one of the major forms. It has been suspected that there exists an initial intermediate, G^{SO}, prior to its further oxidation to G^{SO2} and G^{SO3}, but G^{SO} has never been observed. Using density functional theory, we have explored the energetics and intermediates of 6-TG and $^1O_2$. A new mechanism via $G^{SOOH} \rightarrow G^{SO2} \rightarrow G^{SO4} \rightarrow G^{SO3}$ has been discovered to be the most feasible energetically, whereas the anticipated G^{SO} mechanism is found to encounter an inaccessibly high barrier and thus is prevented. The mechanism through the G^{SOOH} and G^{SO4} intermediates can be validated further by joint experimental measurements, where the fast rate constant of 4.9×10^9 M^{-1} s^{-1} and the reaction stoichiometry of 0.58 supports this low-barrier new mechanism. In addition to the dominant pathway of $G^{SOOH} \rightarrow G^{SO2} \rightarrow G^{SO4} \rightarrow G^{SO3}$, a side pathway with higher barrier, $G^{SOOH} \rightarrow G$, has also been located, providing a rationalization for the observed product distributions of G^{SO2} and G^{SO3} as major products and G as minor product. From mechanistic and kinetics points of view, the present findings provide new chemical insights to understand the high phototoxicity of 6-TG in DNA and point to methods of using 6-TG as a sensitive fluorescence probe for the quantitative detection of $^1O_2$, which holds particular promise for detecting $^1O_2$ in DNA-related biological surroundings.

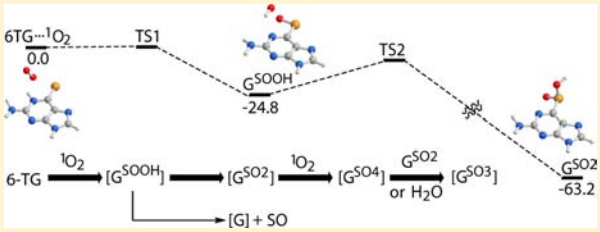

INTRODUCTION

The thiopurines 6-mercaptopurine (6-MP), azathioprine, and 6-thioguanine (6-TG) have been used widely as immunosuppressant, anticancer, and antiinflammatory drugs.[1] They are all prodrugs (compounds that the body converts into active drugs) that are integrated into DNA as 6-TG by metabolism.[2−4] Research shows that patients who undergo years of treatment of thiopurine drugs and sunshine exposure have a 50- to 200-fold increased rate of skin cancer, which is related to the unusual photochemical properties of 6-TG.[5,6] Unlike normal DNA molecules that only absorb UVC and UVB light, 6-TG is a photosensitizer strongly absorbing UVA and a source of reactive oxygen species (ROS),[3,4,6−8] which cause extensive oxidative damage to DNA and proteins.[7−11]

The mechanisms by which DNA 6-TG acts as a UVA photosensitizer and provides a source of promutagenic oxidative DNA damage has attracted strong research interest in recent years.[4,6−8,12] The major ROS generated upon UVA irradiation of 6-TG was identified to be singlet oxygen $^1O_2$.[6,12,13] The oxidation of 6-TG itself by $^1O_2$ constitutes one of the major forms of DNA damage caused by UVA photoactivation of DNA 6-TG.[6,7,12] The successive formation of guanine-6-sulphinate (G^{SO2}) and guanine-6-sulfonate (G^{SO3}) was found to be the major products of free 6-TG reacting with $^1O_2$ (see Scheme 1). Guanine (G) was also identified as a detectable minor product. Formation of the fully oxidized product G^{SO3} is of great significance biologically because the photochemical reactions of 6-TG were shown to be largely context-independent and high yields of G^{SO3} were also formed following UVA irradiation of 6-TG in oligodeoxynucleotides and double-stranded DNA.[7,12] It was shown that G^{SO3} could not form stable base pairs with any normal DNA base and the formation of G^{SO3} will strongly block DNA replication and transcription and become a major factor increasing the risk for skin cancer.[4,6,7,12]

Although the products and conditions have been well established in previous work and despite the strong interest of the scientific community in how these products are formed, the reaction mechanisms accounting for the promutagenic

Scheme 1. Structures of 6-TG and Its Oxidation Products

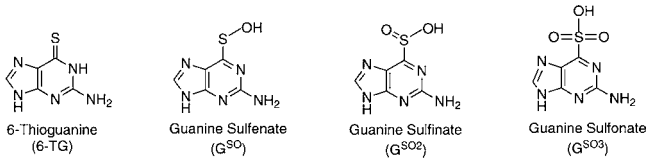

Received: January 15, 2013
Published: February 27, 2013

oxidation product formation from 6-TG with $^1O_2$ remains intriguing and unresolved. One of the main questions lies in whether there exists an initial unstable partially oxidized intermediate, guanine sulfenate (G^{SO}, see Scheme 1), prior to its further oxidation to G^{SO2} and G^{SO3} as suspected before,[6,12] because the postulated intermediate G^{SO} has never been observed. The absence of G^{SO} in experimental detections[6,12] may be due to its instability or indicate different unknown reaction mechanisms leading to G^{SO2} and G^{SO3} formation, which requires further exploration.

On the other hand, the major product of 6-TG with $^1O_2$, G^{SO3}, was found to be highly fluorescent,[6,7] and this motivated us to propose a scheme using 6-TG as a sensitive fluorescence probe for $^1O_2$. It has been essential to develop sensitive and specific $^1O_2$ probes for its importance in understanding $^1O_2$-associated biological functions and photodynamic therapy.[14,15] Much would be gained if $^1O_2$ could be directly monitored. To realize this new method of probing $^1O_2$, it is essential to understand how 6-TG reacts with $^1O_2$ and to determine its reaction stoichiometry.

In pursuing answers to these questions, we performed joint theoretical and experimental investigations on the complex reaction of 6-TG with $^1O_2$. Using density functional theory, a powerful method in dissecting reaction mechanisms, we have explored the energetics and intermediates for the reaction. The peroxy intermediate G^{SOOH}, instead of the previously postulated G^{SO}, is discovered to be the key initial intermediate leading to G^{SO2}. Subsequent to the facile formation of G^{SO2}, two energetically favorable pathways forming G^{SO3} have been located. The experimentally measured reaction stoichiometry and rate constant coincide with theoretical predictions, indicating together a new mechanism leading to the promutagenic oxidation product G^{SO3} and pointing to methods of applying water-soluble 6-TG as a sensitive probe for quantitatively detecting $^1O_2$. By closely coupling the theoretically predicted mechanisms with previous and current experimental observations, the present results provide mechanistic and kinetics insights to understand the high phototoxicity of 6-TG in DNA.

EXPERIMENTAL AND THEORETICAL METHODS

Materials. 6-Thioguanine (Alfa Aesar), Rose Bengal (Alfa Aesar), 9,10-dimethylanthracene (DMA, TCI), and sodium azide (Beyotime Institute of Biotechnology) were used as received. Ultrapure water obtained by Millipore filtration was used as solvent.

Detection of the Rate Constant for 6-TG and $^1O_2$. The third harmonic (355 nm) of a Continuum Surelite II Nd/YAG laser was used to irradiate 6-TG to generate $^1O_2$ and initiate the 6-TG reaction with $^1O_2$. The reaction rate constant of 6-TG with $^1O_2$ was determined by a fluorometric method using the competitive reactions between 6-TG with $^1O_2$ and sodium azide with $^1O_2$.[16] A sample solution containing 30 μM 6-TG and NaN_3 (0–0.4 mM) was irradiated in 1 cm cuvettes, with the beam diverged 355 nm laser at 1 mJ. The fluorescence intensity of G^{SO3} from 6-TG reacting with $^1O_2$ was monitored in the absence and the presence of the physical quencher of $^1O_2$, NaN_3. Fluorescence emission spectra were obtained using a HITACHI f-4600 fluorescence spectrophotometer.

Stoichiometry Measurement for 6-TG and $^1O_2$. The second harmonic (532 nm) of a Continuum Surelite II Nd/YAG laser was used to irradiate DMA–Rose Bengal (5/20 μM) solution or a 6-TG–Rose Bengal (5/20 μM) solution in 1 cm cuvettes, with the beam diverged, and the energy maintained at 1 mJ. Samples were irradiated for a predetermined time and analyzed immediately after irradiation. Fluorescence emission spectra were obtained using a HITACHI f-4600 fluorescence spectrophotometer.

Calculation Methods. The geometries and energies of the reactants, products, intermediates, and transition states were calculated using the hybrid density functional theory (B3LYP) with the standard basis sets of 6-311+G**,[17,18] which is usually a sufficient and affordable computational method for the current system with a commensurate size of two 6-TG molecules. The harmonic frequency analysis was performed to identify the stationary point as either local minima (reactant, products, and intermediates) or first-order saddle points (transition states) and to extract zero-point vibrational energy corrections. Connections of the transition states between two local minima have been confirmed by intrinsic reaction coordinate calculations at the same level.[19] Bulk solvation effects were simulated by using the polarized continuum model (PCM) at the same level.[20] All the calculations were carried out using the Gaussian 09 program package.[21] We also tested other normally adapted density functionals, BP86 and PBE, in connection with 6-311+G** basis sets, but the obtained energies are less reasonable than the B3LYP/6-311+G** results (see the Supporting Information for details). It has been justified that the B3LYP/6-311+G** level of calculation can provide accurate results for nucleic acid bases and base pairs,[22] with including sufficient diffuseness and angular flexibility in the basis sets employed.

RESULTS AND DISCUSSIONS

To elucidate the reaction mechanisms, the potential energy profiles toward G^{SO3} formation were first explored by density functional theory at the B3LYP/6-311+G** level in vacuum and with the bulk solvent effect (H_2O) simulated by the PCM. The optimized structures of reactants, intermediates, transition states, and products are shown in the Supporting Information (Figure S1). The single-point energies are listed in Table S1–S4 (Supporting Information), which show that the energies calculated in vacuum generally do not change much after considering the bulk solvation effect under the PCM. Only some of the barrier heights are lowered in solvents. The hydrogen-bonding effect of the solvent water is also considered in the calculations (Figure S2 and Table S5, Supporting Information) but has been found to have a negligible effect changing the reaction pathways. This is reasonable for the addition reaction of $^1O_2$ to the sulfur atom of 6-TG, where the reaction coordinate is centered on the sulfur atom and the hydrogen-bonded water molecules are far away from the reaction coordinate and mainly serve as spectators. All calculations deal with the neutral form of the related species (shown in Scheme 1) because the initial reactant 6-TG (pK_a = 8.2)[23] exists as the neutral form in aqueous solution at pH = 7.

The potential energy profiles are presented in Figures 1 and 2. As shown in Figure 1, the reactant 6-TG and $^1O_2$ forms a complex 6-TG···$^1O_2$ via a weak hydrogen bond initially, which is followed by the $^1O_2$ bonding with the sulfur atom and the simultaneous hydrogen abstraction by the dangling oxygen atom from the neighboring NH moiety, leading to the formation of the peroxy intermediate G^{SOOH} with an S–O–O–H geometry. It turns out that the cleavage of the weak O–O bond of G^{SOOH} does not result in the anticipated intermediate G^{SO} but leads to G^{SO2} (via TS2) instead, because the departing OH group bonds with the sulfur atom naturally. These calculations indicate that the peroxy intermediate G^{SOOH} is formed prior to G^{SO2}, instead of the previously postulated G^{SO}, as the key intermediate in the initial reaction of 6-TG with $^1O_2$. Thus, the G^{SO2} formation mechanism is modified as 6-TG + $^1O_2$ → G^{SOOH} → G^{SO2} and shown in Scheme 2. Basically, the formation of G^{SO2} is almost barrierless and occurs easily at room temperature because TS1 is only 0.1 kcal mol^{-1} above the reactants and TS2 is lower in energy than the reactants. In addition, G^{SO2} lies 63.2 kcal mol^{-1} below the reactant complex,

dx.doi.org/10.1021/ja400483j | J. Am. Chem. Soc. 2013, 135, 4509–4515

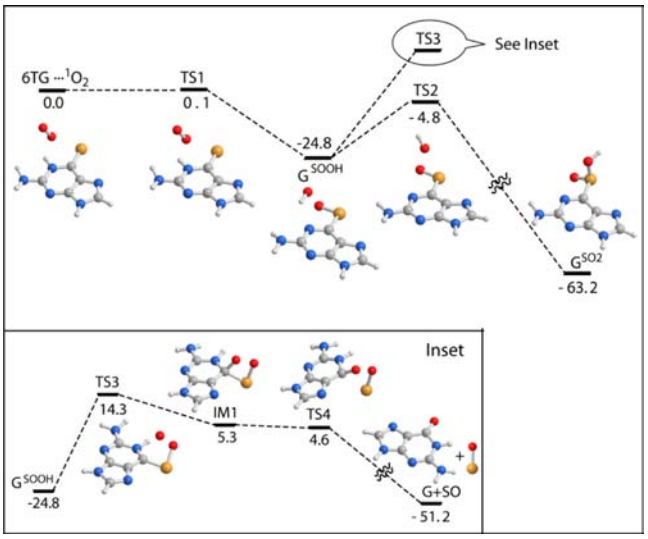

Figure 1. Potential energy profiles for the 6-TG reaction with $^1O_2$ toward the formation of the partially oxidized product G^{SO2} and the minor product G. The energies (in kcal mol^{-1}) are obtained at the B3LYP/6-311+G** level with the solvent effect simulated by PCM. All energies given are relative to the reactant complex of 6-TG with $^1O_2$. Carbon, oxygen, nitrogen, sulfur, and hydrogen atoms are denoted with gray, red, blue, yellow, and white balls, respectively.

indicating its stability. The calculated results corroborate the previous experimental observation[12] that G^{SO2} is one of the major stable products from 6-TG and $^1O_2$.

In competition with G^{SO2} formation, another pathway leading to the stable product G has also been located. As shown in the inset of Figure 1, the departing OH group of G^{SOOH} can also undergo an addition to the carbon atom of the C═S bond, forming a four-membered (OCSO) ring intermediate IM1. The C═S bond in IM1 is thus weakened, and the cleavage of the C═S bond leads to product G. The pathway forming G is rate-limited by the high barrier for the OH addition step (from G^{SOOH} to TS3), which is much higher than the G^{SO2} formation from G^{SOOH}. This result rationalizes the experimental observation that G was detected only as a quite minor product compared to the major oxidized product G^{SO2}.[6,12] TS3 actually lies 14.3 kcal mol^{-1} above the reactant complex (6-TG···$^1O_2$), which means that the pathway forming G is rate-limited by an overall barrier of 14.3 kcal mol^{-1}. So, it is still likely for the energetic reactants to surmount this barrier during thermal fluctuation, resulting in the product G with a detectable low yield at room temperature. The other possible pathway, G^{SO2} reacting with H_2O forming G, has also been located (Figure S3, Supporting Information) but is found to have an inaccessibly high barrier of 35.2 kcal mol^{-1} and can be ruled out as a possibility accounting for the G formation at room temperature.

Following the facile formation of G^{SO2}, further oxidation toward G^{SO3} can still occur, due to the unsaturated bonding valence of the sulfur atom and the high reactivity of $^1O_2$. As a relatively stable primary product, G^{SO2} can serve as the reactant and be extensively involved in subsequent oxidation reaction steps. Three pathways leading to the fully oxidized product G^{SO3} have been located, which are all preceded by the formation of G^{SO2} (Figure 2). In pathway 1, addition of singlet oxygen to G^{SO2} leads to G^{SO4}, overcoming a low barrier of 8.7 kcal mol^{-1}. The intermediate G^{SO4} is quite reactive. The oxygen

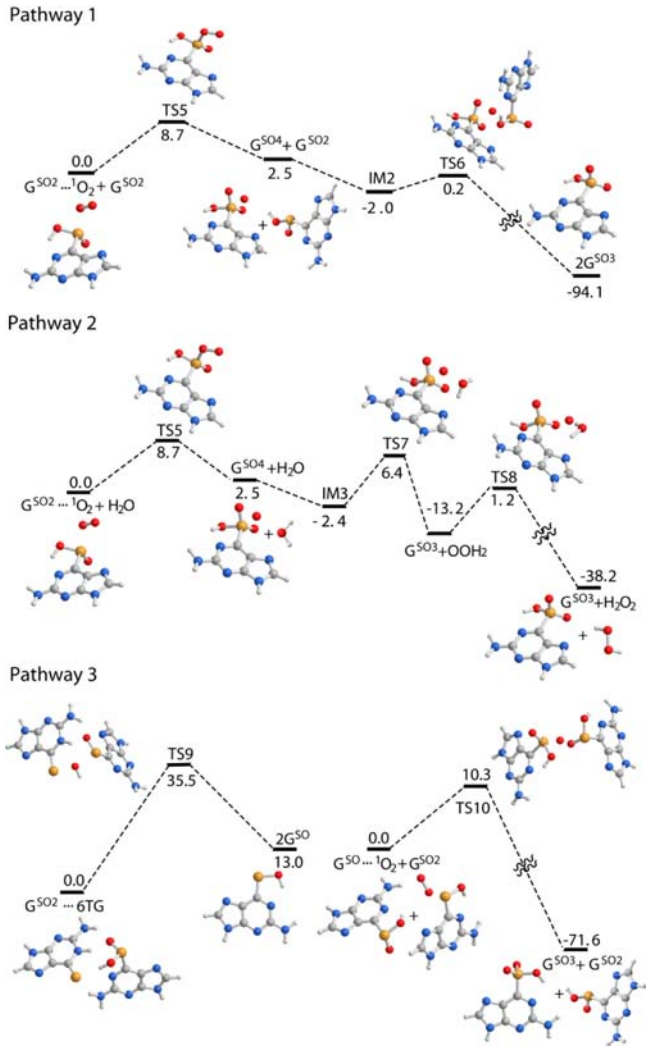

Figure 2. Potential energy profiles for the formation of the fully oxidized major product G^{SO3}, preceded by the intermediate of G^{SO2}. The energies (in kcal mol^{-1}) are obtained at the B3LYP/6-311+G** level with the solvent effect simulated by PCM. All energies given are relative to the reactant complexes of different pathways. Carbon, oxygen, nitrogen, sulfur, and hydrogen atoms are denoted with gray, red, blue, yellow, and white balls, respectively.

Scheme 2. Elucidated Reaction Mechanisms for 6-TG with $^1O_2$[a]

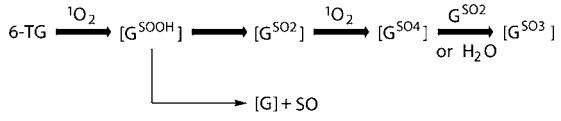

[a]The more favorable reaction pathways are shown with bold arrows.

atom in G^{SO4} can be easily abstracted by another G^{SO2}, forming two G^{SO3} molecules via a low barrier of 2.2 kcal mol^{-1} (from IM2 to TS6). G^{SO3} is the most stable final product that is refractory to further oxidation, because it falls around the global minimum of the potential energy surface with a formation heat of 94.1 kcal mol^{-1} below the reactant complex of G^{SO2}···$^1O_2$. Pathway 1 can be summarized as 2[6-TG] + 3[$^1O_2$] → 2[G^{SO2}] + $^1O_2$ → G^{SO4} + G^{SO2} → 2[G^{SO3}] (see Scheme 2). The whole pathway involves two 6-TG molecules and three singlet oxygen molecules and yields two G^{SO3} molecules. Considering the low

dx.doi.org/10.1021/ja400483j | J. Am. Chem. Soc. 2013, 135, 4509−4515

barrier of 8.7 kcal mol^{-1} forming G^{SO4} as the rate-limiting step, it is expected that pathway 1 can take place favorably.

Once G^{SO4} is formed as in pathway 1, another route is open for the formation of G^{SO3}, through the participation of water molecules. H_2O can form a hydrogen-bonded complex (IM3) with G^{SO4}, through which the oxygen atom in G^{SO4} is abstracted by H_2O via TS7, yielding the stable product G^{SO3} and H_2O_2. This constitutes pathway 2 and can be summarized as 6-TG + $2[^1O_2] \rightarrow G^{SO2} + {}^1O_2 \rightarrow G^{SO4} + H_2O \rightarrow G^{SO3} + H_2O_2$ (See scheme 2 and Figure 2). One 6-TG molecule, one H_2O molecule, and two $^1O_2$ molecules are involved, yielding one G^{SO3} molecule and one H_2O_2 molecule in this mechanism. In pathway 2, only low barriers of 8.7 kcal mol^{-1} (for the G^{SO4} formation step) and 6.4 kcal mol^{-1} (from reactant to TS7) are involved, and considering the use of aqueous solution as reaction medium, the ubiquitous presence of water molecules may greatly facilitate this pathway.

The third located pathway involves the formation of the previously anticipated G^{SO} intermediate. But, unlike the proposed mechanism before,[6,12] the calculations show that G^{SO} can not be formed directly from 6-TG and $^1O_2$. The initial intermediate formed by $^1O_2$ addition to 6-TG is the peroxy intermediate G^{SOOH}, and the O−O bond dissociation of G^{SOOH} only results in the formation of G^{SO2} but not G^{SO}, as has been illustrated in Figure 1. So, other possibilities forming G^{SO} were explored. Due to its relative stability, G^{SO2} is susceptible to further reactions, which might lead to G^{SO}. As shown in Figure 2 (pathway 3), another 6-TG molecule may abstract the OH group from G^{SO2} and produce two G^{SO} molecules. But, such a reaction requires overcoming a barrier of 35.5 kcal mol^{-1}, indicating that the formation of G^{SO} is energetically inaccessible at room temperature. Even with the aid of a H_2O molecule, this pathway still has a high barrier of 33.6 kcal mol^{-1} (Figure S3, Supporting Information).We then calculated the subsequent reaction of G^{SO}. It shows that G^{SO} is reactive and susceptible to further oxidation by $^1O_2$. Addition of $^1O_2$ to G^{SO}, when catalyzed by another G^{SO2}, yields G^{SO3} with a barrier of 10.3 kcal mol^{-1}. Pathway 3 can be summarized as $2[6\text{-TG}] + {}^1O_2 \rightarrow G^{SO2} + 6\text{-TG} \rightarrow 2G^{SO} + 2{}^1O_2 + G^{SO2} \rightarrow 2G^{SO3} + G^{SO2}$ (see Figure 2). This pathway is rate-limited by the high barrier of 35.5 kcal mol^{-1} for the G^{SO} formation step and thus is unlikely to occur, compared to the energetically favorable pathways 1 and 2.

Overall, the energetically accessible pathways for the reaction of 6-TG with $^1O_2$ can be summarized in Scheme 2. The branching of the reaction flux takes place in the intermediate G^{SOOH}. From G^{SOOH}, a predominant formation of G^{SO2} over G formation is expected, according to the calculated potential energy profiles in Figure 1. Once G^{SO2} is formed, the subsequent oxidation to G^{SO3} takes place readily. So, according to the calculated pathways, the successive formation of G^{SO2} and G^{SO3} is expected to predominate that of the product G, which explains the product distributions[6,12] that G^{SO2} and G^{SO3} were observed as major products and G as minor product. In addition, the calculated results can provide rationale for the previously reported absence of the anticipated intermediate G^{SO} in experimental detections.[12] In the serial experiments,[6,12] G^{SO3} was first detected as the fully oxidized product and suggested to be formed via the successive intermediates, G^{SO} and G^{SO2} (as shown in Scheme 1), but only G^{SO2} was separated and identified as a relatively stable intermediate in UVA-mediated 6-TG oxidation, which could be further oxidized to G^{SO3}. The likely initial intermediate G^{SO} has never been observed. It was suspected that G^{SO} is unstable under the experimental condition.[12] From the calculated reaction pathways here, it shows that the peroxy intermediate G^{SOOH} is formed as the initial intermediate for the reaction of 6-TG with $^1O_2$ and G^{SOOH} leads to G^{SO2} instead of G^{SO}. Another possible pathway forming G^{SO} encounters a high barrier of 35.5 kcal mol^{-1}, indicating that the G^{SO} mechanism has little possibility to be involved and contribute to the final G^{SO3} formation. Instead, the newly discovered pathways 1 and 2 forming G^{SO3} via the successive intermediates of G^{SOOH}, G^{SO2}, and G^{SO4} (Scheme 2) only require surmounting much lower barriers (8.7 kcal mol^{-1}) and thus are energetically more favorable. Altogether, these results indicate a new plausible mechanism forming G^{SO3} via $G^{SOOH} \rightarrow G^{SO2} \rightarrow G^{SO4} \rightarrow G^{SO3}$, rather than the anticipated mechanism through the intermediates of G^{SO} and G^{SO2}. Also, it clarifies why no G^{SO} was able to be detected previously.

To validate the reaction mechanisms predicted by the above theoretical calculations, we performed further experiments to measure the reaction rate constant and stoichiometry. The measurement will also provide quantitative kinetics data, which remains unknown up to now. First, the reaction rate constant of 6-TG with $^1O_2$ was determined by a fluorometric method[16] using the competitive reactions between 6-TG with $^1O_2$ and sodium azide with $^1O_2$. $^1O_2$ was produced through photosensitization of 6-TG by 355 nm irradiation in air-saturated aqueous solution and reacted with 6-TG itself to produce the fluorescent product G^{SO3}. The fluorescence intensity of G^{SO3} from 6-TG reacting with $^1O_2$ was monitored in the absence and the presence of the physical quencher of $^1O_2$, NaN_3. The reaction rate constant of 6-TG and $^1O_2$ was then obtained on the basis of eq 1, where I_0/I is the ratio of the fluorescence intensity of product G^{SO3} in the absence and the presence of NaN_3, k_T and k_q are the rate constants for the 6-TG and $^1O_2$ reaction and the NaN_3 and $^1O_2$ reaction, respectively, k_d is the decay rate of $^1O_2$ in aqueous solution, and [T] and [Q] are the concentrations of 6-TG and NaN_3, respectively. k_q and k_d are known:[25,26]

$$\frac{I_0}{I} = 1 + \frac{k_q}{k_T[T] + k_d}[Q] \quad (1)$$

As shown in Figure 3, the fluorescence intensity of G^{SO3} decreases when the concentrations of sodium azide increase. The Stern−Volmer plot of the fluorescence intensity against NaN_3 concentration (inset of Figure 3) shows good linearity, from which the reaction rate constant of 6-TG and $^1O_2$ forming G^{SO3} is calculated to be 4.9×10^9 M^{-1} s^{-1}. The fast rate measured here verifies further the theoretically elucidated mechanisms in Scheme 2. As revealed in the calculations (Figure 2), only low barriers (8.7 kcal mol^{-1}) are encountered along pathways 1 and 2 for the predicted mechanisms forming G^{SO3} via $G^{SOOH} \rightarrow G^{SO2} \rightarrow G^{SO4} \rightarrow G^{SO3}$, while the G^{SO} mechanism (pathway 3) involves a much higher barrier of 35.5 kcal mol^{-1}. Consequently, the observed fast formation rate of G^{SO3} supports the $G^{SOOH} \rightarrow G^{SO2} \rightarrow G^{SO4} \rightarrow G^{SO3}$ mechanism, instead of the G^{SO} mechanism.

Additional experiments were performed to measure the reaction stoichiometry of 6-TG with $^1O_2$. A fluorescent singlet oxygen probe, DMA, which can react with $^1O_2$ in a 1:1 stoichiometry to form a nonfluorescent product, was used as a reference reaction.[14] $^1O_2$ was produced by 532 nm irradiation of Rose Bengal and reacted separately with DMA and 6-TG

dx.doi.org/10.1021/ja400483j | J. Am. Chem. Soc. 2013, 135, 4509−4515

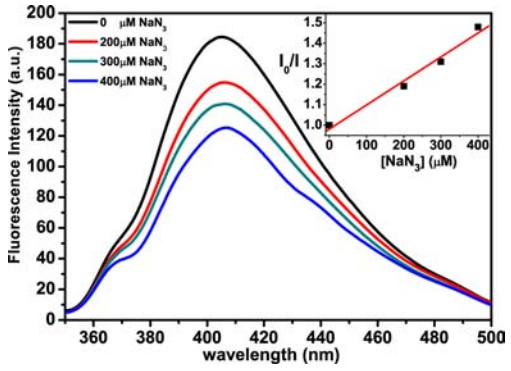

Figure 3. Fluorescence spectra taken for the air-saturated aqueous solution of 6-TG (30 μM) with NaN_3 (0–0.4 mM) after 355 nm irradiation for 3 min. $^1O_2$ was generated by UVA photosensitization of 6-TG, reacting with 6-TG itself to yield the fluorescent product G^{SO3} in the system. The excitation wavelength for fluorescence measurements was 320 nm. These fluorescence emission spectra (peak at 408 nm, λ_{em} = 408 nm) and excitation spectra (Figure S4, Supporting Information) match those reported for G^{SO3}.[24] Inset: the Stern–Volmer plot of the fluorescence intensity of G^{SO3} in the absence (I_0) and the presence (I) of the $^1O_2$ quencher, NaN_3.

under identical experimental conditions. In these experiments, DMA and 6-TG do not absorb 532 nm and only react separately with the $^1O_2$ produced by 532 nm photosensitization of Rose Bengal, because no fluorescence change was observed under nitrogen-saturated conditions. The reaction of 6-TG or DMA with $^1O_2$ proceeds linearly with irradiation time, as reflected by the fluorescence intensity change with time (plotted in Figures 4 and 5). The absolute quantity of singlet

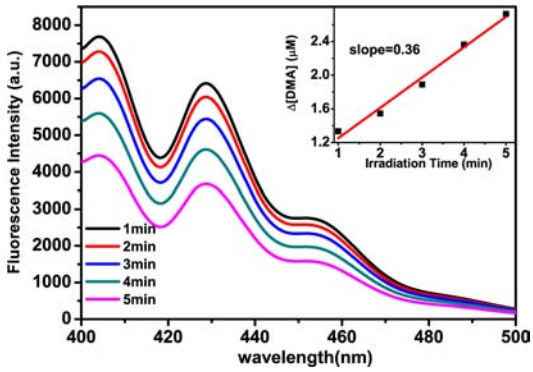

Figure 4. Fluorescence spectra of DMA (λ_{ex} = 390 nm, λ_{em} = 428 nm) taken for air-saturated solutions of DMA–Rose Bengal (5/20 μM) after different irradiation times at 532 nm, which reflect the time course of the DMA reaction with $^1O_2$. The inset plots Δ[DMA] versus irradiation time, derived from the fluorescence spectra. The line is linear best-fits to the data.

oxygen is unknown in these systems, but it increases proportionally with the irradiation time, so the irradiation time can be taken as the relative concentration of $^1O_2$. The inset of Figure 4 shows a plot of Δ[DMA] versus irradiation time derived from the photolysis experiments and reveals the consumption of [DMA] versus the relative concentration of $^1O_2$, which has a linear relationship with a slope of about 0.36. Similarly, the consumption of [6-TG] versus the relative concentration of $^1O_2$ is also obtained (inset of Figure 5), which exhibits good linearity with a slope of 0.21. The ratio of these two slopes (0.21/0.36 = 0.58) represents the stoichiometry

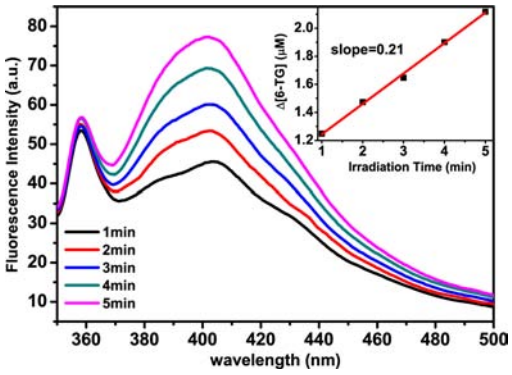

Figure 5. Fluorescence spectra of G^{SO3} (λ_{ex} = 320 nm, λ_{em} = 408 nm) taken for air-saturated solutions of 6-TG–Rose Bengal (5/20 μM) after different irradiation times at 532 nm, which reflect the time course of the 6-TG reaction with $^1O_2$. The inset plots Δ[6-TG] versus irradiation time, derived from the fluorescence spectra. The line is linear best-fits to the data. The peak at ~360 nm is the Raman scattering band of the solvent water, which does not vary with the irradiation time. The product concentration of G^{SO3} is smaller than that in Figure 3, as reflected by the lower fluorescence intensity. So, the Raman band of water is obvious in Figure 5. But, the Raman band is well separated from the fluorescence band of G^{SO3}, so it does not interfere with the spectral analysis.

ratio of the 6-TG and $^1O_2$ versus the DMA and $^1O_2$ reactions. Since it is known that one DMA molecule reacts with one $^1O_2$ molecule, the stoichiometry of 6-TG and $^1O_2$ is thus derived to be 0.58.

According to our calculation, G^{SO3} is formed most feasibly through the $G^{SOOH} \rightarrow G^{SO2} \rightarrow G^{SO4} \rightarrow G^{SO3}$ mechanism via pathways 1 and 2 (Figure 2). For pathway 1, two 6-TG molecules react with three $^1O_2$ molecules and produce two G^{SO3} molecules, which should correspond to a stoichiometry of 0.67 (2/3 = 0.67). Likewise, a stoichiometry of 0.5 could be anticipated for pathway 2 because one 6-TG molecule, one H_2O molecule, and two $^1O_2$ molecules are involved in this pathway to yield one G^{SO3}. If the reaction follows both pathway 1 and pathway 2, it can be predicted that the reaction stoichiometry for G^{SO3} formation lies between 0.5 and 0.67. Indeed, the obtained stoichiometry of 0.58 from our measurements turns out to be an average of the two predicted values, corroborating further the $G^{SOOH} \rightarrow G^{SO2} \rightarrow G^{SO4} \rightarrow G^{SO3}$ mechanism through both pathways 1 and 2. Meanwhile, the stoichiometry of 0.58 confirms the participation of water as a reactant as in pathway 2, because the reaction stoichiometry should be 0.67 if only 6-TG and $^1O_2$ are reactants leading to G^{SO3} as in pathway 1.

The current $G^{SOOH} \rightarrow G^{SO2} \rightarrow G^{SO4} \rightarrow G^{SO3}$ mechanism forming G^{SO3} via both pathways 1 and 2 is suitable for the free 6-TG molecules reacting with $^1O_2$. By extrapolating this mechanism to DNA-embedded 6-TG, it is expected that pathway 1 based on two 6-TG molecules has little probability to occur, because the 6-TG concentration is very small in the DNA of patients treated with thiopurines (≤0.05% of DNA G).[4,5] So, pathway 2, which involves a single reacting 6-TG, is the more plausible mechanism accounting for G^{SO3} formation in the patients treated with thiopurine drugs. Moreover, pathway 2 generates G^{SO3} together with a molecule of H_2O_2, another ROS, which may induce extra DNA damage and thus has important implications.

On the basis of the above mechanistic and kinetics studies, we discuss the potential applications of 6-TG as a fluorescence

dx.doi.org/10.1021/ja400483j | J. Am. Chem. Soc. 2013, 135, 4509–4515

probe for $^1O_2$. Quantitative detection of small amounts of $^1O_2$ is currently difficult in aqueous solution under physiological conditions, where the lifetime of $^1O_2$ is very short.[27] So, it has been essential to develop fluorescence probe molecules that can react with $^1O_2$ faster than the decay rate of $^1O_2$ in an aqueous solution ($k_d = 2.4 \times 10^7$ s^{-1}).[26] We show here that 6-TG can react with $^1O_2$ rapidly at 4.9×10^9 M^{-1} s^{-1}, faster than the well-known sensitive $^1O_2$ fluorescence probe DMA (2×10^7 to 9×10^8 M^{-1} s^{-1}, refs 28−30). In addition, the strongly fluorescent product G^{SO3} (excitation maximum = 324 nm, emission maximum = 408 nm) is formed on top of the negligible fluorescence background of 6-TG. These advantages render 6-TG a new sensitive $^1O_2$ fluorescence probe. Furthermore, with the stoichiometry of G^{SO3} from 6-TG and $^1O_2$ determined here (0.58), it is expected that the concentration of $^1O_2$ could be obtained by monitoring the fluorescence intensity of G^{SO3}. This could even enable quantitative detection of $^1O_2$ by using 6-TG as a fluorescence probe.

CONCLUSION

In summary, our investigation demonstrates that the highly reactive oxidation of 6-TG by $^1O_2$ toward G^{SO3} formation is most likely preceded by the successive intermediates of G^{SOOH}, G^{SO2}, and G^{SO4}, without participation of the anticipated intermediate G^{SO}. Addition of $^1O_2$ to the sulfur atom of 6-TG leads to the initial peroxy intermediate G^{SOOH}, which is followed by the facile formation of G^{SO2}. The further oxidation of G^{SO2} by $^1O_2$ leads to G^{SO4}, and G^{SO4} reacts with G^{SO2} or H_2O to give rise to the most stable oxidation product G^{SO3}. The newly discovered $G^{SOOH} \rightarrow G^{SO2} \rightarrow G^{SO4} \rightarrow G^{SO3}$ mechanisms only involve low barriers (8.7 kcal mol^{-1}) and are the most energetically favorable, whereas the anticipated G^{SO} mechanism turns out to have little possibility to occur because the possible formation pathway of G^{SO} encounters a much higher barrier that is energetically infeasible (35.5 kcal mol^{-1}). In addition to the dominant pathway of $G^{SOOH} \rightarrow G^{SO2} \rightarrow G^{SO4} \rightarrow G^{SO3}$, a side pathway with higher barrier (14.3 kcal mol^{-1}), $G^{SOOH} \rightarrow G$, has also been located.

The predicted $G^{SOOH} \rightarrow G^{SO2} \rightarrow G^{SO4} \rightarrow G^{SO3}$ mechanisms are further validated by joint experimental measurements on reaction stoichiometry and rate constant. The measured fast rate constant of 4.9×10^9 M^{-1} s^{-1} supports the low barrier $G^{SOOH} \rightarrow G^{SO2} \rightarrow G^{SO4} \rightarrow G^{SO3}$ mechanism, rather than the G^{SO} mechanism that encounters an inaccessibly high barrier. The obtained stoichiometry of 0.58 is an average of the predicted values for the two energetically favorable pathways of the $G^{SOOH} \rightarrow G^{SO2} \rightarrow G^{SO4} \rightarrow G^{SO3}$ mechanism, corroborating further such a mechanism. The reaction rate constant and stoichiometry measured here also supply quantitative kinetics data for the reaction of 6-TG and $^1O_2$.

The newly discovered reaction mechanisms can clarify why no G^{SO} was able to be detected before and rationalize the observed product distributions of G^{SO2} and G^{SO3} as major products and G as minor product. The low barriers and fast reaction rate constants revealed here explain the high reactivity of $^1O_2$ oxidizing 6-TG. From mechanistic and kinetics points of view, the present findings provide new chemical insights to understand the high phototoxicity of 6-TG in DNA and the increased incidence of skin cancer upon UVA light exposure in patients treated with thiopurine drugs. The measured reaction rate and stoichiometry also point to new approaches of using 6-TG as a sensitive fluorescence probe for the quantitative detection of $^1O_2$, which holds particular promise for detecting $^1O_2$ in DNA-related biological surroundings because 6-TG can be easily integrated into DNA.

ASSOCIATED CONTENT

Supporting Information

Optimized structures and their Cartesian coordinates for reactants, intermediates, transition states, and products, table of the energies for all these structures in vacuum and in water, as well as other calculated results for comparison. This material is available free of charge via the Internet at http://pubs.acs.org.

AUTHOR INFORMATION

Corresponding Author

hongmei@iccas.ac.cn

Notes

The authors declare no competing financial interest.

ACKNOWLEDGMENTS

This work was financially supported by the National Natural Science Foundation of China (grant no. 21073201), the National Basic Research Program of China (2013CB834602), and the CAS Water Science Project. The calculations were supported by the Supercomputing Center, Computer Network Information Center of Chinese Academy of Sciences.

REFERENCES

(1) Aarbakke, J.; JankaSchaub, G.; Elion, G. B. *Trends Pharmacol. Sci.* **1997**, *18*, 3−7.
(2) Waters, T. R.; Swann, P. F. *Biochemistry* **1997**, *36*, 2501−2506.
(3) Hofbauer, G. F. L.; Attard, N. R.; Harwood, C. A.; McGregor, J. M.; Dziunycz, P.; Iotzova-Weiss, G.; Straub, G.; Meyer, R.; Kamenisch, Y.; Berneburg, M.; French, L. E.; Wuthrich, R. P.; Karran, P.; Serra, A. L. *Am. J. Transplant.* **2012**, *12*, 218−225.
(4) Brem, R.; Karran, P. *Photochem. Photobiol.* **2012**, *88*, 5−13.
(5) Euvrard, S.; Kanitakis, J.; Claudy, A. *N. Engl. J. Med.* **2003**, *348*, 1681−1691.
(6) Zhang, X. H.; Jeffs, G.; Ren, X. L.; O'Donovan, P.; Montaner, B.; Perrett, C. M.; Karran, P.; Xu, Y. Z. *DNA Repair* **2007**, *6*, 344−354.
(7) O'Donovan, P.; Perrett, C. M.; Zhang, X. H.; Montaner, B.; Xu, Y. Z.; Harwood, C. A.; McGregor, J. M.; Walker, S. L.; Hanaoka, F.; Karran, P. *Science* **2005**, *309*, 1871−1874.
(8) Brem, R.; Li, F.; Karran, P. *Nucleic Acids Res.* **2009**, *37*, 1951−1961.
(9) Brem, R.; Daehn, I.; Karran, P. *DNA Repair* **2011**, *10*, 869−876.
(10) Gueranger, Q.; Kia, A.; Frith, D.; Karran, P. *Nucleic Acids Res.* **2011**, *39*, 5057−5066.
(11) Daehn, I.; Brem, R.; Barkauskaite, E.; Karran, P. *FEBS Lett.* **2011**, *585*, 3941−3946.
(12) Ren, X. L.; Li, F.; Jeffs, G.; Zhang, X. H.; Xu, Y. Z.; Karran, P. *Nucleic Acids Res.* **2010**, *38*, 1832−1840.
(13) Zhang, Y. Z.; Zhu, X. C.; Smith, J.; Haygood, M. T.; Gao, R. M. *J. Phys. Chem. B* **2011**, *115*, 1889−1894.
(14) Gomes, A.; Fernandes, E.; Lima, J. *J. Biochem. Biophys. Methods* **2005**, *65*, 45−80.
(15) Hirakawa, K. *Anal. Bioanal. Chem.* **2009**, *393*, 999−1005.
(16) Song, B.; Wang, G. L.; Tan, M. Q.; Yuan, J. L. *J. Am. Chem. Soc.* **2006**, *128*, 13442−13450.
(17) Lee, C. T.; Yang, W. T.; Parr, R. G. *Phys. Rev. B* **1988**, *37*, 785−789.
(18) Becke, A. D. *J. Chem. Phys.* **1993**, *98*, 5648−5652.
(19) Gonzalez, C.; Schlegel, H. B. *J. Phys. Chem.* **1990**, *94*, 5523−5527.
(20) Mennucci, B.; Tomasi, J. *J. Chem. Phys.* **1997**, *106*, 5151−5158.
(21) Frisch, M. J.; et al. *Gaussian 09*, revision B.01; Gaussian, Inc.: Wallingford, CT, 2009.

(22) (a) Wesolowski, S. S.; Leininger, M. L.; Pentchev, P. N.; Schaefer, H. F. *J. Am. Chem. Soc.* **2001**, *123*, 4023−4028. (b) Li, X. F.; Cai, Z. L.; Sevilla, M. D. *J. Phys. Chem. B* **2001**, *105*, 10115−10123. (c) Kumar, A.; Sevilla, M. D. *J. Phys. Chem. B* **2009**, *113*, 11359−11361.
(23) Fox, J. J.; Wempen, I.; Hampton, A.; Doerr, I. L. *J. Am. Chem. Soc.* **1958**, *80*, 1669−1675.
(24) Finkel, J. M. *J. Pharm. Sci.* **1975**, *64*, 121−122.
(25) Miskoski, S.; García, N. A. *Photochem. Photobiol.* **1993**, *57*, 447−452.
(26) Schmidt, R. *J. Am. Chem. Soc.* **1989**, *111*, 6983−6987.
(27) Schweitzer, C.; Schmidt, R. *Chem. Rev. (Washington, DC, U. S.)* **2003**, *103*, 1685−1758.
(28) Corey, E. J.; Taylor, W. C. *J. Am. Chem. Soc.* **1964**, *86*, 3881−3882.
(29) Usui, Y. *Chem. Lett.* **1973**, 743−744.
(30) Wilkinson, F.; Helman, W. P.; Ross, A. B. *J. Phys. Chem. Ref. Data* **1995**, *24*, 663−1021.